

Synchrotron-Based Chemical Nano-Tomography of Microbial Cell-Mineral Aggregates in their Natural, Hydrated State

Gregor Schmid,¹ Fabian Zeitvogel,¹ Likai Hao,¹ Pablo Ingino,¹ Wolfgang Kuerner,¹ James J. Dynes,² Chithra Karunakaran,² Jian Wang,² Yingshen Lu,² Travis Ayers,³ Chuck Schietinger,³ Adam P. Hitchcock,⁴ and Martin Obst^{1,*}

¹Department of Geosciences, Center for Applied Geoscience, University of Tuebingen, Hoelderlinstr. 12, 72074 Tuebingen, Germany

²Canadian Light Source Inc., Saskatoon, Canada

³Luxel Corp., Friday Harbor, USA

⁴McMaster University, Hamilton, Canada

Abstract: Chemical nano-tomography of microbial cells in their natural, hydrated state provides direct evidence of metabolic and chemical processes. Cells of the nitrate-reducing *Acidovorax* sp. strain BoFeN1 were cultured in the presence of ferrous iron. Bacterial reduction of nitrate causes precipitation of Fe(III)-(oxyhydr)oxides in the periplasm and in direct vicinity of the cells. Nanoliter aliquots of cell-suspension were injected into custom-designed sample holders wherein polyimide membranes collapse around the cells by capillary forces. The immobilized, hydrated cells were analyzed by synchrotron-based scanning transmission X-ray microscopy in combination with angle-scan tomography. This approach provides three-dimensional (3D) maps of the chemical species in the sample by employing their intrinsic near-edge X-ray absorption properties. The cells were scanned through the focus of a monochromatic soft X-ray beam at different, chemically specific X-ray energies to acquire projection images of their corresponding X-ray absorbance. Based on these images, chemical composition maps were then calculated. Acquiring projections at different tilt angles allowed for 3D reconstruction of the chemical composition. Our approach allows for 3D chemical mapping of hydrated samples and thus provides direct evidence for the localization of metabolic and chemical processes *in situ*.

Key words: chemical tomography, hydrated, bacteria, STXM, soft X-rays, 3D

INTRODUCTION

In the last decade there have been substantial advances in three-dimensional (3D) microscopy approaches such as laser scanning and electron microscopy (EM) in the fields of life, environmental, and material science. The limiting factor, in particular when analyzing soft, biological matter, often is sample preparation. Conventional EM preparation techniques focus on the preservation of the (ultra-)structure of the sample when the sample is exposed to the vacuum environment. In contrast, light or laser scanning microscopy approaches are capable of analyzing samples in their natural, hydrated state, but with moderate spatial resolution only. Both approaches are limited regarding their information content on the chemical composition of the sample.

These limitations were overcome with the development of the synchrotron-based spectromicroscopy approach of scanning transmission (soft) X-ray microscopy (STXM). One of the major advantages is the capability of using the intrinsic X-ray absorption properties of samples to create image contrast without adding any heavy metal stains or fluorescence probes, and of direct quantitative mapping of chemical species. This is achieved by combining a ~30 nm spatial resolution nanoprobe

with the chemical speciation capabilities of near edge X-ray absorption fine structure spectroscopy (NEXAFS). Samples can be analyzed in various environments from vacuum, special atmospheres, to fully hydrated samples in thin, aqueous layers (Bluhm et al., 2006). In the latter approach, samples are sandwiched in a 1–2 μm thick layer of water between two Si_3N_4 membranes. Recently, STXM angle-scanning tomography was developed to obtain chemical information on thin, bio-, geo-, environmental and material science samples both in dry and wet environments (Hitchcock, 2012). Si_3N_4 sandwich wet cells are incompatible with high tilt angles in STXM because of geometrical constraints (Fig. 1). Thus, samples for wet STXM tomography were previously mounted as aqueous suspensions in μm diameter glass capillaries (Johansson et al., 2006). Limitations of this approach are insufficient immobilization resulting in below-optimum spatial resolution when the sample is exposed to high acceleration (several G) during sample scanning, and the high X-ray absorption by the glass capillaries.

Here, we describe a novel approach of analyzing hydrated samples that are mounted between two LUXFilm® membranes (Luxel, Friday Harbor, USA) that keep the sample both hydrated and rigidly immobilized. The wet cells allow for a sample rotation of $\pm 72^\circ$ around the length axis in a conventional STXM setup. This allowed for data acquisition and 3D reconstruction of the distribution of

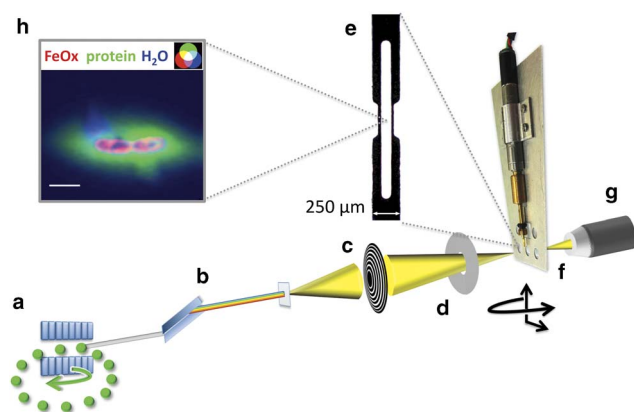


Figure 1. Schematic of synchrotron-based scanning transmission X-ray microscopy chemical nano-tomography. A synchrotron-based (a) monochromatic soft X-ray beam (b) is focused using a zone plate (c). Second and higher order light is blocked by the order-sorting aperture (d). The sample mounted in a wet cell (e) is scanned through the focused spot from different angles (f). The distance between aperture (d) and focus is typically a few $100\ \mu\text{m}$, and thus limiting the sample size that can be rotated without collision to a few $100\ \mu\text{m}$ perpendicular to the rotation axis, which is incompatible with conventional wet cells of several mm in width. Transmission (g) images are converted into quantitative, chemically specific maps (h). Scale bar is $1\ \mu\text{m}$.

protein and Fe-(oxyhydr)oxides in a hydrated cell-mineral aggregate formed by nitrate-reducing, Fe(II)-oxidizing bacteria. A spatial resolution of at least $50\ \text{nm}$ in the reconstruction was obtained. The overall goal of this development is to better understand the mechanisms of microbial Fe(II)-oxidation by *Acidovorax*, the spatial distribution of the resulting Fe-biominerals, and its influence on the sequestration of heavy metals in the environment (Hitchcock et al., 2012). This novel tomography approach provides a powerful new tool for the 3D chemical analysis of thin bio-, geo-, and environmental samples in their natural, hydrated state.

MATERIALS AND METHODS

Cell Cultivation

Cells of the nitrate-reducing *Acidovorax* sp. strain BoFeN1 isolated from anoxic freshwater sediments of Lake Constance were cultured under anoxic conditions as described previously (Kappler et al., 2005). In brief, cells were grown for 7 days in anoxic freshwater medium in the presence of $10\ \text{mM}$ Fe(II)Cl₂, $10\ \text{mM}$ nitrate and $5\ \text{mM}$ acetate. The cell suspension was sampled with a 1 mL syringe, centrifuged, and re-suspended in Fe(II)-free medium.

Wet cell loading

A 1 mL syringe with cell suspension was mounted into a custom-made portable nano-injector (Fig. 2) and connected via silicone tubing to a $5\ \mu\text{m}$ glass micropipette (TW100-4, WPI, Sarasota, FL, USA). The micropipette was mounted to



Figure 2. Portable nano-injector for 1 mL syringes, built from a micrometer gauge.

a three axis linear translation stage (Newport, Bozeman, MT, USA) that allowed for precisely punching two holes (inlet, outlet) through the upper membrane of a custom-designed STXM tomography wet cell (Luxel, Friday Harbor, USA). The wet cell (Fig. 1e) consists of a metal frame that is coated from both sides with $30\ \text{nm}$ LUXFilm®. Nanoliters of the cell suspension were then injected between the membranes. The polymer films collapsed around bacteria and small cell-mineral aggregates by capillary forces and thereby both sealed the wet cell against drying and immobilized the samples for scanning. The previously punched holes were closed with nail polish.

Tomography Stage

The wet cell was mounted onto a $0.8\ \text{mm}$ diameter brass rod that was flat on one end. The rod was mounted onto a custom-made tomography stage (Fig. 1f), that was built from a stepper motor (Faulhaber ADM0620, Faulhaber, Schoenaich, Germany) equipped with a planetary gearhead with a reduction rate of 1,024:1 resulting in a theoretical angle resolution of $0.0176^\circ/\text{step}$. The rod mounting mechanism was adapted from an earlier version of a STXM tomography stage (Johansson et al., 2007).

STXM Data Acquisition

The tomography stage was mounted onto the piezo scanning stage of the STXM at beamline 10ID-1 at the Canadian Light Source Inc. (CLS) (Kaznatcheev et al., 2007). The microscope chamber was not evacuated of air to prevent rapid evaporation, but flushed with He, which is X-ray transparent. After identifying areas of interest, images were acquired at three specific energies across the O 1s absorption edge (528 , 532.2 , and $538.3\ \text{eV}$) and at two specific energies across the Fe 2p absorption edge (705 and $723.8\ \text{eV}$). Images were acquired across an angle range of $\pm 72^\circ$ in 4° steps.

Reconstruction

The image sequences consisting of three and two images at the O 1s and the Fe 2p absorption edges, respectively were aligned individually for each absorption edge and rotation angle, and converted from transmission to linear absorbance [optical density (OD)] scale using the tools implemented in the software package aXis2000 (Hitchcock, 2013) as described

in detail elsewhere (Dynes et al., 2006). Species-specific maps were then calculated by subtracting the pre-edge absorbance from images acquired at X-ray energies with high specificity for certain chemical species. The image difference map $OD_{723.8\text{ eV}} - OD_{705.0\text{ eV}}$ is specific for the Fe(III)-(oxyhydr)oxide. Chemical maps were also obtained by linear decomposition (Koprinarov et al., 2002) by fitting the absorbance at selected energies with those obtained from reference spectra of albumin, water, ferrihydrite and a modeled, nonspecific background based on the atomic scattering factors (Henke et al., 1993). For example, the absorbance at 532.2 eV is dominated by excitation of the $1s \rightarrow \pi^*$ transition at the C = O in the peptide bond. The protein map contains minor contributions of other organic carbon species such as polysaccharides. No pixels of the resulting fits contained negative values within the cell-mineral aggregate area. For practical reasons, the measurements of the I_0 signal for the conversion into linear absorbance were done inside the wet cell area adjacent to the sample. As a result, the water layer was normalized out by the conversion. Fitting using the atomic scattering factors (Henke et al., 1993), however, showed a homogeneous water layer of ~ 120 nm in the analyzed area that allowed for an easy correction of the water map for 2D presentation. The 3D reconstruction was done without the featureless 120 nm water layer and thus only shows differences in water thickness. The resulting chemical maps were aligned. The 3D reconstruction was done using the software package IMOD employing the simultaneous iterative reconstruction technique (SIRT) algorithm with 400 iterations (Kremer et al., 1996). For visualization the software package Chimera (Pettersen et al., 2004) was used. Schmid and Obst (2013) provide a more detailed description of STXM tomography including mounting of dry samples, data acquisition, and reconstruction. To verify the hydrated state of the sample, an image sequence across the O 1s absorption edge was acquired with a spectral sampling of 0.2 eV steps in the spectral region of interest. To avoid radiation damage to the cells examined in the area of interest, other pristine bacterial cells were used. The image stack was fitted with previously described reference spectra that were normalized to a nominal thickness of 1 nm using the atomic scattering factors (Henke et al., 1993) and an assumed density. A more detailed description of the spectromicroscopic fitting approach including precision and fitting error estimations was published by Dynes et al. (2006).

RESULTS AND DISCUSSION

Quantitative 3D reconstructions of the three chemical species “water,” “protein,” and “Fe-(oxyhydr)oxide” acquired at the O 1s edge and of the “Fe-(oxyhydr)oxide” acquired at the Fe 2p edge are presented in Figure 3 as projection images. The respective 3D datasets can be downloaded as 3D-movies from the Supplementary Movie 1. The spatial distribution of the Fe-precipitates mapped at both the O 1s (Fig. 3a) and the Fe 2p (Fig. 3d) edges are similar. The maps of the individual chemical species allow for the identification of the 3D spatial arrangement of the Fe-precipitates produced by

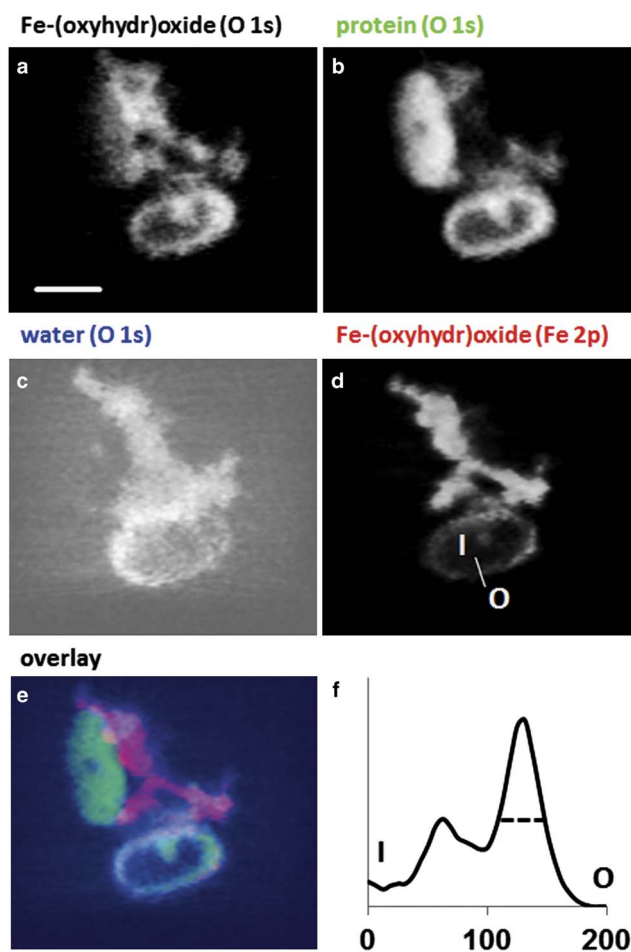


Figure 3. Projection images of chemically specific three-dimensional datasets acquired at the O 1s edge (a–c), Fe 2p edge (d) and an overlay (e) of hydrated *Acidovorax* sp. strain BoFeN1 bacteria in the stage of precipitating Fe(III)-(oxyhydr)oxide. The line profile (shown in d) across the Fe-precipitate encrusted periplasm (f) shows a thickness of ~ 40 nm (full-width at half-maximum). I, inside cell; O, outside cell. Scale bar is 500 nm.

the nitrate-reducing, Fe(II)-oxidizing bacteria in their native, hydrated state at a spatial resolution of <50 nm.

Supplementary Movie 1

Supplementary Movie 1 can be found online. Please visit journals.cambridge.org/jid_MAM.

Extracellular Fe-precipitates can be distinguished clearly from the rim of Fe-precipitates in the periplasm, i.e. between the inner and the outer membranes (Fig. 3a). The upper, left cell shows a rather homogeneous distribution of protein (Fig. 3b). This cell does not appear in the Fe 2p-derived dataset (Fig. 3d) as the periplasm does not contain Fe-(oxyhydr)oxides, in contrast with the lower cell that shows a rim of Fe-(oxyhydr)oxides in the periplasm. In contrast to previous studies of air-dried samples (Miot et al., 2009) for the first time we could preserve nonencrusted cells that were neither chemically or cryo-fixed (Miot et al., 2011). In keeping with the

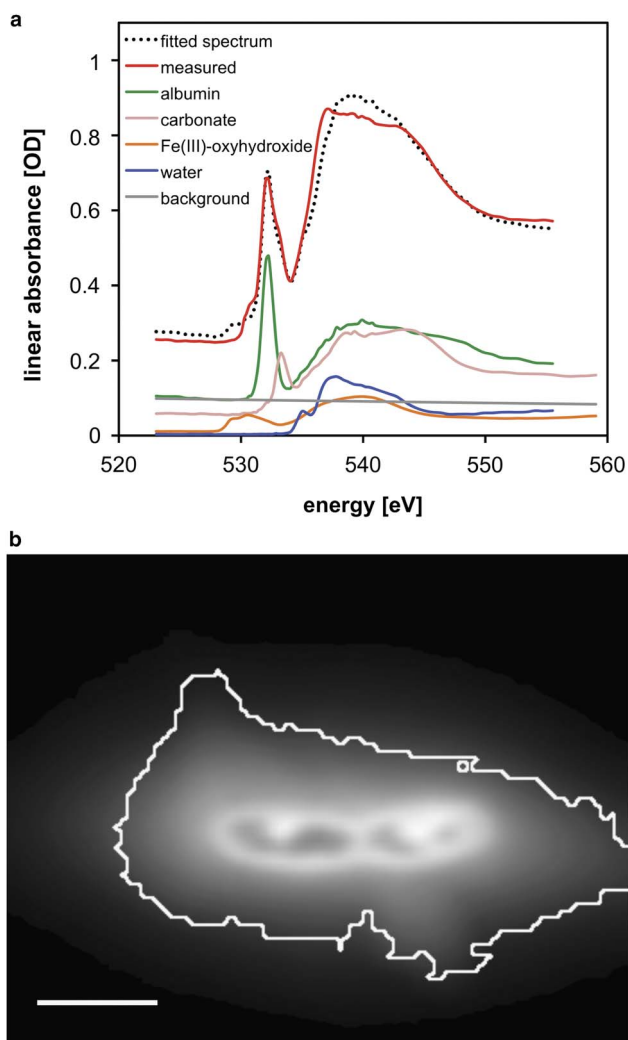


Figure 4. a: Curve fitting of the average O 1s spectrum with spectra of well-characterized reference compounds. The measured spectrum was extracted from the area outlined in (b). Scale bar is 1 μm .

above-mentioned previous studies, in the periplasm of the encrusted, lower cell, a close association of the Fe-precipitates with protein can be observed (Fig. 3e), whereas the extracellular Fe-precipitates seem to contain less protein.

Figure 3f shows a profile of the Fe-(oxyhydr)-oxide distribution of the lower cell, that clearly showed a rim-like structure. The full-width at half-maximum (FWHM) of the absorption profile across this rim-like structure is in the range of 35–50 nm.

The measured average O 1s absorption spectrum of the area of the two hydrated cells in the wet cell is presented in Figure 4a. Different combinations of reference spectra (protein, xanthan, water, goethite, ferrihydrite, and siderite as a proxy for carbonate) were tested. The least residuals in a linear fit were obtained using a combination of protein (Stewart-Ornstein et al., 2007), water (kindly provided by V. Berejnov), ferrihydrite, and carbonate. By linear decomposition, average thicknesses of 400, 32, 11, and 40 nm were calculated for protein, water, ferrihydrite, and carbonate, respectively, within the whole region of interest (ROI).

As mentioned previously in the Material and Methods section, an additional 120 nm of water has to be added, which results in an efficient total water thickness of ~ 250 nm in the cell region.

Sample Immobilization, Spatial Resolution and Restrictions on Sample Geometry

The rigid immobilization of the sample by the polyimide membrane that collapsed around the cell-mineral aggregate allowed for 3D analysis of features such as the Fe-(oxyhydr) oxide layer in the periplasm with a FWHM of 35–50 nm, which is consistent with previous transmission electron microscopy results (Miot et al., 2011). These were the smallest structural features observed in our sample. From its FWHM we estimated a resolution of at least 50 nm. A decrease of spatial resolution in the z -direction is because of the effect of limited tilt angle ($\pm 72^\circ$) in angle-scan tomography as the wet cell-structure would obscure the beam at higher angles (Midgley & Weyland, 2003). Considering the 40 nm diffraction-limited resolution of the zone plate and the 25 nm pixel spacing, our *in situ* STXM tomography approach obviously was not limited by sample mounting, by vibrations during sample scanning, or by sample movement. These are considered to be the major advantages compared with previous approaches wherein wet samples were analyzed in water-filled glass capillaries (Johansson et al., 2006). Even higher spatial resolutions as compared with the results of this study should be possible if zone plates with smaller outermost zone width and thus smaller X-ray spot size are used (Thompson et al., 2009)—the record spatial resolution in STXM is presently 10 nm (Chao et al., 2012). However the focal length decreases as the outermost zone width decreases and thus increased spatial resolution may lead to smaller depths of field and potential geometrical problems of rotating the 250 μm wide wet cell in very close proximity to the order-sorting aperture (Fig. 1d). Furthermore, as STXM is operated in a transmission setup requiring soft X-ray transparency, the sample geometry is restricted to thin samples. Single bacteria (≈ 1 μm thickness and few 100 nm of effective thickness, e.g., *BoFeN1*, $l \approx 2$ μm , $w \approx 500$ nm, effective thickness 400 nm of protein) and thin biofilms are well suited for STXM in both 2D and 3D measurements (Dynes et al., 2006; Johansson et al., 2006; Hunter et al., 2008; Miot et al., 2009; Wang et al., 2011). Thicker samples, however, cannot be analyzed due to problems with absorption saturation (Hanhan et al., 2009). Typical maximum effective thickness values depend on the density and range from ~ 300 nm at the C 1s edge (284 eV) to 1–2 μm at higher energies such as the Si 1s edge (1,839 eV).

X-ray Induced Radiation Damage

Radiation-induced damage in STXM tomography depends on the sensitivity of the chemical species analyzed and needs to be estimated for each case individually. However, in STXM tomography beam-damage is approximately an order of magnitude lower than in full field transmission X-ray microscopy (Hitchcock, 2012) where the detection efficiency

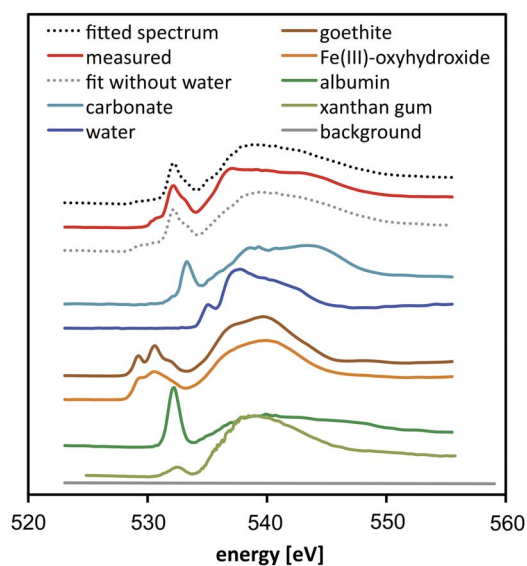


Figure 5. Average O 1s spectrum (red) of the ROI marked in Figure 4 and fits with (black dots) and without (gray dots) water included. All spectra of the reference compounds that were used for the fittings are illustrated above.

is lower by at least an order of magnitude because of the presence of an inefficient imaging micro-zone plate after the sample. Potential mechanisms of radiation-induced damage at the O 1s edge would be the break of chemical bonds and the formation of radicals. Both mechanisms could result potentially in a decrease of the protein signal at 532.2 eV. Other effects might be beam-induced oxidation or reduction of redox-sensitive species. These influences can be quantified by comparative measurements at the respective specific X-ray energies before, and after the tomography acquisition, or by monitoring the specific absorbance at specific energies within a rotation series. In our study, no significant changes in absorbance at 532.2 eV from the beginning to the end of the rotation series were observed.

Spectroscopic Proof of Hydrated State

Spectroscopic measurements at the O 1s edge proved that the 30 nm LUXFilm[®] polymer membranes were able to keep the sample hydrated during the measurement. Whereas the homogeneous “background” water signal was normalized out for practical reasons (see Methods section), thickness variations in the region of the aggregate allowed for extracting the spectral features typical for liquid water. The linear fit of the acquired O 1s spectra using characterized reference materials (Fig. 5) shows the measured spectrum could not be fit to similar quality without water (i.e., 15% increase of standard deviation of the fit).

Data Acquisition Times

Since STXM is a raster-scanning approach, acquisition times critically depend on the size of area scanned and on the selected pixel spacing. The area that can be analyzed by STXM tomography is somewhat limited horizontally by the

depth of field, which results in defocusing effects for large sample widths at high tilt angles. In this study at the O 1s and the Fe 2p edges, using a zone plate with 40 nm outermost zone width, an aggregate of $\sim 1.5 \mu\text{m}$ width was scanned in a $3 \times 3 \mu\text{m}^2$ frame with 120×120 pixels with dwell times of 1 ms/pixel. Defocusing effects because of the depth of field were not observed even at relatively high tilt angles such as $\pm 60^\circ$. Data acquisition times were ~ 6 min/rotation angle at the O 1s edge (three different X-ray energies) plus an additional 5 min at the Fe 2p edge (two different energies). Of these 11 min/angle step only ~ 4 min were used to acquire the five images; the remainder of the time was required for rotation, localization, focusing, and energy stepping. A full rotation dataset ($\pm 72^\circ$ at 4° step size) with five X-ray energies was acquired in ~ 8 h.

Outlook: Next Generation STXM

Automated re-localization and focusing after each rotation step would drastically reduce acquisition times. Next generation STXMs such as the instrument at beamline 5.3.2.1 (Kilcoyne et al., 2010) at the ALS (Advanced Light Source, Berkeley, USA) are capable of moving the focused spot by scanning the zone plate instead of the sample stage. This might allow for using eucentric rotation stages commonly used for EM or transmission X-ray microscopy (TXM) beamlines so that the data acquisition could potentially be automated similar to modern TXM tomography beamlines, but retaining the advantage of higher detection efficiency and thus reduced beam-damage as well as the high energy resolution and ease of photon energy scanning of modern STXM beamlines.

SUMMARY AND CONCLUSIONS

We show 3D reconstructions of the chemical composition of bacterial cell-mineral aggregates, in their natural, hydrated state with < 50 nm spatial resolution. This approach is a powerful tool for bio-, geo-, and environmental science since it can provide direct evidence of linkages between metabolic and chemical processes and the resulting 3D distribution of chemical species such as metabolites or precipitates, without artifacts from sample drying.

ACKNOWLEDGMENTS

We thank the Geomicrobiology Group of A. Kappler (University of Tuebingen), E. Struve, and V. Berejnov (for providing H₂O spectrum). Project funding: DFG Emmy-Noether fellowship to M.O. (OB 362/1-1). The CLS is supported by NSERC, CIHR, NRC, the Province of Saskatchewan, WEDC, and the University of Saskatchewan. 3D rendering done using UCSF Chimera package developed by the RBVI at UCSF (supported by NIGMS P41-GM103311).

REFERENCES

- BLUHM, H., ANDERSSON, K., ARAKI, T., BENZERARA, K., BROWN, G.E., DYNES, J.J., GHOSAL, S., GILLES, M.K., HANSEN, H.C., HEMMINGER, J.C., HITCHCOCK, A.P., KETTELER, G., KILCOYNE, A.L.D., KNEEDLER, E.,

- LAWRENCE, J.R., LEPPARD, G.G., MAJZLAN, J., MUN, B.S., MYNENI, S.C.B., NILSSON, A., OGASAWARA, H., OGLETTREE, D.F., PECHER, K., SALMERON, M., SHUH, D.K., TONNER, B., TYLISZCZAK, T., WARWICK, T. & YOON, T.H. (2006). Soft X-ray microscopy and spectroscopy at the molecular environmental science beamline at the advanced light Source. *J Electron Spectrosc* **150**(2–3), 86–104.
- CHAO, W., FISCHER, P., TYLISZCZAK, T., REKAWA, S., ANDERSON, E. & NAULLEAU, P. (2012). Real space soft x-ray imaging at 10 nm spatial resolution. *Opt Express* **20**(9), 9777–9783.
- DYNES, J.J., TYLISZCZAK, T., ARAKI, T., LAWRENCE, J.R., SWERHON, G.D. W., LEPPARD, G.G. & HITCHCOCK, A.P. (2006). Speciation and quantitative mapping of metal species in microbial biofilms using scanning transmission X-ray microscopy. *Environ Sci Technol* **40**(5), 1556–1565.
- HANHAN, S., SMITH, A.M., OBST, M. & HITCHCOCK, A.P. (2009). Optimization of analysis of soft X-ray spectromicroscopy at the Ca 2p edge. *J Electron Spectrosc* **173**(1), 44–49.
- HENKE, B.L., GULLIKSON, E.M. & DAVIS, J.C. (1993). X-ray interactions—Photoabsorption, scattering, transmission, and reflection at E = 50–30,000 eV, Z = 1–92. *Atom Data Nucl Data* **54**(2), 181–342.
- HITCHCOCK, A.P. (2012). Soft X-ray imaging and spectromicroscopy. In *Handbook of Nanoscience*, van Tendeloo, G., van Dyck, D. & Pennycook, S.J. (Eds.), pp. 745–791. Weinheim: Wiley-VCH Verlag GmbH & Co. KGaA.
- HITCHCOCK, A.P. (2013). aXis2000 Is an IDL-Based Analytical Package. Available at <http://unicorn.mcmaster.ca/aXis2000.html>, free of charge for non-commercial use.
- HITCHCOCK, A.P., OBST, M., WANG, J., LU, Y.S. & TYLISZCZAK, T. (2012). Advances in the detection of as in environmental samples using low energy X-ray fluorescence in a scanning transmission X-ray microscope: Arsenic immobilization by an Fe(II)-oxidizing freshwater bacteria. *Environ Sci Technol* **46**(5), 2821–2829.
- HUNTER, R.C., HITCHCOCK, A.P., DYNES, J.J., OBST, M. & BEVERIDGE, T.J. (2008). Mapping the speciation of iron in *Pseudomonas aeruginosa* biofilms using scanning transmission X-ray microscopy. *Environ Sci Technol* **42**(23), 8766–8772.
- JOHANSSON, G.A., DYNES, J.J., HITCHCOCK, A.P., TYLISZCZAK, T., SWERHON, G.D. & LAWRENCE, J.R. (2006). Chemically sensitive tomography at 50 nm spatial resolution using a soft X-ray scanning transmission X-ray microscope. *Microsc Microanal* **12** (S02), 1412.
- JOHANSSON, G.A., TYLISZCZAK, T., MITCHELL, G.E., KEEFFE, M.H. & HITCHCOCK, A.P. (2007). Three-dimensional chemical mapping by scanning transmission X-ray spectromicroscopy. *J Synchrotron Radiat* **14**(Pt 5), 395–402.
- KAPPLER, A., SCHINK, B. & NEWMAN, D.K. (2005). Fe(III) mineral formation and cell encrustation by the nitrate-dependent Fe(II)-oxidizer strain BoFeN1. *Geobiology* **3**(4), 235–245.
- KAZNATCHEEV, K.V., KARUNAKARAN, C., LANKE, U.D., URQUHART, S.G., OBST, M. & HITCHCOCK, A.P. (2007). Soft X-ray spectromicroscopy beamline at the CLS: Commissioning results. *Nucl Instrum Meth A* **582**(1), 96–99.
- KILCOYNE, D., ADE, H., ATTWOOD, D., HITCHCOCK, A., MCKEAN, P., MITCHELL, G., MONTEIRO, P., TYLISZCZAK, T. & WARWICK, T. (2010). A new scanning transmission X-ray microscope at the ALS for operation up to 2500 eV. *AIP Conf Proc* **1234**(1), 465–468.
- KOPRINAROV, I.N., HITCHCOCK, A.P., MCCRORY, C.T. & CHILDS, R.F. (2002). Quantitative mapping of structured polymeric systems using singular value decomposition analysis of soft X-ray images. *J Phys Chem B* **106**(21), 5358–5364.
- KREMER, J.R., MASTRONARDE, D.N. & MCINTOSH, J.R. (1996). Computer visualization of three-dimensional image data using IMOD. *J Struct Biol* **116**(1), 71–76.
- MIDGLEY, P.A. & WEYLAND, M. (2003). 3D electron microscopy in the physical sciences: the development of Z-contrast and EFTEM tomography. *Ultramicroscopy* **96**(3–4), 413–431.
- MIOT, J., BENZERARA, K., MORIN, G., KAPPLER, A., BERNARD, S., OBST, M., FERARD, C., SKOURI-PANET, F., GUIGNER, J.M., POSTH, N., GALVEZ, M., BROWN, G.E. & GUYOT, F. (2009). Iron biomineralization by anaerobic neutrophilic iron-oxidizing bacteria. *Geochim Cosmochim Acta* **73**(3), 696–711.
- MIOT, J., MACLELLAN, K., BENZERARA, K. & BOISSET, N. (2011). Preservation of protein globules and peptidoglycan in the mineralized cell wall of nitrate-reducing, iron(II)-oxidizing bacteria: a cryo-electron microscopy study. *Geobiology* **9**(6), 459–470.
- PETTERSEN, E.F., GODDARD, T.D., HUANG, C.C., COUCH, G.S., GREENBLATT, D.M., MENG, E.C. & FERRIN, T.E. (2004). UCSF Chimera—A visualization system for exploratory research and analysis. *J Comput Chem* **25**(13), 1605–1612.
- SCHMID, G. & OBST, M. (2013). 3D chemical mapping: Application of scanning transmission (soft) X-ray microscopy (STXM) in combination with angle-scan tomography in bio-, geo- and environmental science. In *Methods in Molecular Biology: Electron Microscopy*, Kuo, J. (Ed.), pp. 757–781. Springer New York: Humana Press.
- STEWART-ORNSTEIN, J., HITCHCOCK, A.P., CRUZ, D.H., HENKLEIN, P., OVERHAGE, J., HILPERT, K., HALE, J.D. & HANCOCK, R.E.W. (2007). Using intrinsic X-ray absorption spectral differences to identify and map peptides and proteins. *J Phys Chem B* **111**(26), 7691–7699.
- THOMPSON, A.C., ATTWOOD, D., GULLIKSON, E., HOWELLS, M., KIM, K.J., KIRZ, J., KORTRIGHT, J., LINDAU, I., LIU, Y., PIANETTA, P., ROBINSON, A., SCOFIELD, J., UNDERWOOD, J., WILLIAMS, G. & WINICK, H. (2009). X-ray properties of the elements. In *X-Ray Data Booklet*, Thompson, A.C. (Ed.), pp. 1–53. Berkeley: Lawrence Berkeley National Laboratory.
- WANG, J., HITCHCOCK, A.P., KARUNAKARAN, C., PRANGE, A., FRANZ, B., HARKNESS, T., LU, Y., OBST, M. & HORMES, J. (2011). 3D chemical and elemental imaging by STXM spectrotomography. In *AIP Conference Proceedings* **1365**, McNulty, I., Eyberger, C. & Lai, B. (Eds.), pp. 215–218. New York: AIP Publishing.